THE JOURNAL OF PHYSICAL CHEMISTRY B

Article

pubs.acs.org/JPCB

Coupled Multimodal Dynamics of Hydrogen-Containing Ion Networks in Water-Deficient, Sodium Hydroxide-Aluminate Solutions

Trent R. Graham,*[,†] David Semrouni,[‡] Eugene Mamontov,[§] Anibal J. Ramirez-Cuesta,[§] Katharine Page,[§] Aurora Clark,[‡,†] Gregory K. Schenter,[†] Carolyn I. Pearce,[†] Andrew G. Stack,[∥] and Hsiu-Wen Wang*[,∥]

[†]Pacific Northwest National Laboratory, Richland, Washington 99352, United States

[‡]Department of Chemistry and the Materials Science and Engineering Program, Washington State University, Pullman, Washington 99164, United States

[§]Neutron Scattering Division and [∥]Chemical Sciences Division, Oak Ridge National Laboratory, Oak Ridge, Tennessee 37831, United States

Supporting Information

ABSTRACT: The (meta)stability of low water activity sodium hydroxide/aluminate ($Na^+OH^-/Al(OH)_4^-$) electrolytes dictates kinetics in the Bayer process for aluminum refining and high-level nuclear waste processing. We utilized quasi-elastic neutron scattering (QENS) and proton nuclear magnetic resonance spectroscopy (^1H NMR) in extremely concentrated sodium aluminate solutions to investigate the picosecond (ps) to microsecond (ms) timescale motions of H-bearing species ($Al(OH)_4^-$ monomers/clusters, OH^- and H_2O). In the QENS data, in contrast to typical liquids, no short-time translational diffusion was observed at 293 K, but two types of localized motions were found: (i) local backbone tumbling or a formation of large hydrated ion clusters on the order of 40−60 ps; and (ii) much slower, complex, and collective dynamics of the ensemble of H-bearing species on the order of 350−750 ps. Variable temperature, pulsed field gradient, and diffusion-ordered ^1H NMR was used to determine the ensemble translational motion along with relaxometry to calculate rotational correlation coefficients. The ensemble rotational correlation times were on the order of 184−300 ps from ^1H NMR, which is consistent with the timescale of the QENS components. Complementary molecular dynamics simulation of NaOH solutions exhibit extensive ion networks potentially responsible for the observed dynamical coupling of water with the motion of large hydrated ion clusters. Understanding these collective motions will aid in predicting the behavior of complex solutions during aluminum production and during nuclear waste processing.

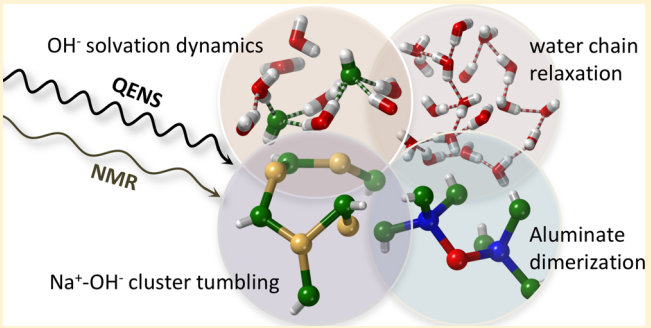

1. INTRODUCTION

Hydration shell dynamics and morphologies are ion-dependent, ranging from a high degree of order in kosmotropic solutions to a hydration shell lacking structure in chaotropic solutions.[1−7] The hydration shell morphology is perturbed at high salt concentrations,[8,9] which can lead to instabilities and concurrent nucleation.[10,11] For example, the lifetime and diffusive motions of ion clusters and disruption of the water hydrogen-bonding network by ion aggregations are also much less understood but are of great importance to a range of materials and chemical processes.[8−11] This perturbed hydration shell also surrounds electrolytes enriched near solid−fluid interfaces and heavily influences interfacial processes.[12] The Bayer process for the recovery of aluminum (Al) from bauxite[13] is another example, in which Na^+ interactions with tetrahedral, monomeric, aluminate anions, $Al(OH)_4^-$, lead to incredibly stable and concentrated electrolytes that can exist at supersaturated conditions for extended periods of time.[14] The high solubility of $Al(OH)_4^-$ in caustic Na^+ electrolytes is also important in high-level radioactive wastes (HLW), where large quantities of sodium hydroxide (NaOH) were initially introduced to dissolve aluminum fuel cladding, neutralize acidic wastes,[15] and continue to be introduced to dissolve aluminum (oxy)hydroxides and stabilize the $Al(OH)_4^-$ ions in solution.

The structure and dynamics of highly alkaline sodium aluminate solutions ($NaOH−NaAl(OH)_4−H_2O$) are poorly understood. As summarized by Sipos,[14] the mechanisms of

Received: September 25, 2018
Revised: November 7, 2018
Published: November 8, 2018

ACS Publications © XXXX American Chemical Society

DOI: 10.1021/acs.jpcb.8b09375
J. Phys. Chem. B XXXX, XXX, XXX−XXX

formation of contact ion pairs comprising $NaOH^{\bullet}$ and $NaAl(OH)_4^{\bullet}$ and their assembly into networks of species are the most unresolved questions in the speciation model of sodium aluminate solutions. In contrast, the structure and dynamics of relatively simple NaOH solutions have been investigated in great detail,[16−21] particularly by recent neural network-based molecular dynamics (MD) simulations.[22−24] At high concentrations, Na^+ exhibits a broad distribution of polyhedral coordinations, wherein H_2O and OH^- are confined to corner-, edge-, or face-sharing sites between multiple Na^+ ions.[20,24] The preference for Na^+ to coordinate with H_2O in dilute conditions (e.g., 92% [5−6 H_2O] at 0.4 *m*) is decreased significantly with increasing NaOH concentrations. Despite the deficiency of solvent water molecules at high NaOH concentrations, Na^+ is still able to retain its weak selectivity toward H_2O, for example, Na^+ on average coordinates to 0−2 OH^- ligands and 4−5 H_2O molecules with total coordination number ranging from 4−7 at saturation (27.7 *m*).[24] The increased OH^- concentrations also influence H_2O and OH^- self-exchange mechanisms around Na^+, where both the "direct" leaving events and "proton transfer-driven" events occur, because hydrogen bonds of water to the OH^- ions effectively aid in moving protons between solvating H_2O to the OH^- ions and back.[22,23] Such proton transfer motions in aqueous hydroxide solutions are believed to be a multiscale and multidynamical process taking place over picosecond time-scales.[21,25,26]

To shed light onto the dynamic nature of hydroxo−aqua complexes and correlated water solvation exchanges, (incoherent) quasi-elastic neutron scattering (QENS) and ^1H nuclear magnetic resonance spectroscopy (^1H NMR) for NaOH−$NaAl(OH)_4$−H_2O at very high ionic concentrations are carried out. These studies explore the "water-in-salt" scenario,[12] where the average number of water molecules available to solvate each Na^+, OH^-, and $Al(OH)_4^-$ is far below the primary solvation numbers, which are well established in dilute conditions. NaOH−H_2O and NaOH−$NaAl(OH)_4$−H_2O solutions with total Na^+ concentration above 20 *m* are investigated here. We seek to understand the dynamic properties of H_2O, OH^-, and $Al(OH)_4^-$ species and their local cooperative motions at temperatures and solution compositions representing idealized brines in HLW storage tanks, albeit omitting the presence of colloidal Al (oxy)-hydroxides and other prevalent Na^+ electrolytes (e.g. sodium nitrate).

2. EXPERIMENT

2.1. Sample Preparation. Sample preparation was performed in an ultra-high purity, Ar-filled glovebox. The Ar environment protects against CO_2 capture known to be significant for concentrated NaOH solutions at ambient conditions. Samples were prepared according to the compositions listed in Table 1. 20 *m* NaOH solution was prepared from commercially available 50 wt % stock solution (Sigma-Aldrich, 3415413) by dilution with a known amount of CO_2-free deionized water. NaOH−$NaAl(OH)_4$−H_2O solutions were generated by quantitative dissolution of degreased Al wire (99.999% grade) in 50 wt % stock NaOH solution, with the removal of water facilitated by evaporation in the glovebox at elevated temperatures or addition of CO_2-free deionized water as needed to achieve the desired total NaOH and $NaAl(OH)_4$ concentrations (see Table 1).

Table 1. Composition of the NaOH−H_2O and NaOH−$NaAl(OH)_4$−H_2O Solutions

	NaOH−H_2O	NaOH−$NaAl(OH)_4$−H_2O	
	NoAl	LowAl	HighAl
	speciation (molal)		
y: NaOH (total)	20.059	18.305	30.008
x: $NaAl(OH)_4$		5.898	9.668
y−*x*: NaOH (ex)	20.059	12.408	20.339
	salt (mole)		
Na^+	20.059	18.305	30.008
Al		5.898	9.668
OH^-	20.059	35.998	59.013
H_2O	55.506	55.506	55.506
	ratio		
$Na^+(ex)/Al(OH)_4^-$		2.10	2.10
$Na^+(tot)/Al(OH)_4^-$		3.10	3.10
$H_2O/Al(OH)_4^-$		9.41	5.74
H_2O/NaOH(ex)	2.77	4.47	2.73

The dissolution of Al wire can be simply expressed according to the following equation

$$x\mathrm{Al}_{(s)} + y\mathrm{NaOH}_{(aq)} + 3x\mathrm{H_2O}_{(aq)} \rightarrow x\mathrm{NaAl(OH)}_{4(aq)} + (y-x)\mathrm{NaOH}_{(aq)} + (3x/2)\mathrm{H}_{2(g)}$$

where the predominate form of Al^{3+} is aluminate $Al(OH)_4^-$. The variable denoted (*y*−*x*) defines the excess amount of NaOH (i.e., free Na^+ and OH^- species) that is not associated with the $Al(OH)_4^-$ monomer [in 1:1 ratio of Na^+ and $Al(OH)_4^-$] and is subject to change with the formation of dimer or polynuclear aluminate complexes. Hereafter, and throughout the rest of the article, we abbreviated the three solutions as: NoAl for the aluminum-free NaOH solution, and LowAl and HighAl for the two sodium aluminate solutions with 5.9 and 9.7 *m* total Al, respectively. Note that the $Na^+/Al(OH)_4^-$ ratios in LowAl and HighAl solutions are equivalent, and they only differ by the degree of dilution. Complementary Raman spectroscopy measurements (details appear in Supporting Information, Section S1) were completed on the LowAl solution, which show characteristic symmetric AlO_4 stretching (from $Al(OH)_4^-$ monomer at 625 cm^{-1}), as well as two weak sidebands (at 545 and 700 cm^{-1}) likely correlated to aluminate dimers/clusters.[14,27]

2.2. Quasi-Elastic (Incoherent) Neutron Scattering. Prepared solutions were sealed into a QENS flat plate, aluminum sample container (0.1 mm gap) with interior walls coated by a 5 μm thick layer of gold to prevent corrosion. QENS data were recorded on the backscattering spectrometer BASIS[28] (Spallation Neutron Source, Oak Ridge National Laboratory, USA), with a scattering wavenumber range Q = 0.3−1.9 $Å^{-1}$, an energy resolution ΔE = 3.5 μeV (full-width at half maximum), and the dynamic energy range E = −100 to +500 μeV. The gold-coated flat aluminum sample container was mounted onto a closed-cycle refrigerator, which controlled the temperature within ±5 K. For each solution, data were collected at T = 273, 293, 313, 333, 353 K, and at 4 K after the series of dynamic measurements. The 4 K data were used to determine the instrument's resolution. Temperature-dependent background scans were acquired of the empty gold-coated sample container and subtracted from the sample data, with the exception of the 4 K scans used to quantify resolution. A dynamic range between −100 and +500 μeV was used in the

DOI: 10.1021/acs.jpcb.8b09375
J. Phys. Chem. B XXXX, XXX, XXX−XXX

data analysis. Incoherent elastic neutron intensity scans were also collected while warming the container from the baseline temperature of about 10 K with a temperature ramp rate of 1 K/min. Complementary temperature-dependent elastic neutron total scattering/radial distribution function analyses were completed for deuterated-equivalent solution at the NOMAD[29] beamline on the HighAl solution to follow any changes in the local atomic structure upon heating. Details appear in Supporting Information Section S2.

2.3. ^{1}H NMR Spectroscopy. Variable temperature, ^{1}H NMR studies were conducted on the sample series on a Varian-Inova, narrow bore NMR spectrometer at a field strength of 17.6 T with the locking field disabled. The temperature was calibrated using ethylene glycol for temperatures between 293 and 353 K and deuterated methanol at 273 K.[30] A 4 mm Teflon insert, coaxially inserted inside a 5 mm gas tight NMR tube, was used for the experiments. Following insertion in the NMR spectrometer, the 90° pulse width was quantified for each sample, at each temperature, using a variable pulse width experiment containing a standard single pulse (pw-*acquisition*). The delay between experiments (d_1) was >5 T_1, known recursively, and this 90° pulse width was used for the following NMR experiments. The ensemble ^{1}H spin lattice relaxation time was quantified with a standard two pulse, inversion recovery experiment (180°−τ−90°−*acquisition*) with a delay between experiments (d_1) > 5 T_1. The ensemble ^{1}H longitudinal relaxation time was quantified with a Hahn echo decay experiment (90°−τ−180°−τ−*acquisition*) with a delay between experiments (d_1) > 5 T_1. Diffusion coefficients were quantified with a gradient compensated stimulated echo with spin lock and convection compensation pulse sequence (DgcsteSL_cc), in which the spatially dependent magnetic field pulse strength was varied in 16 steps typically between 1.8 and 45.3 G cm^{-1} and with a delay between experiments (d_1) > 5 T_1. The spatially dependent magnetic field pulse duration and delay between spatially dependent magnetic field pulses was optimized for between 80 and 95% signal attenuation. The optimized spatially dependent magnetic field pulse duration and delay varied from 10.4 to 2.8 and 85.0 to 30.0 ms, respectively, decreasing in value as the temperature increased. DgcsteSL_cc experiments were calibrated to the known diffusion of trace HOD in D_2O at 25 °C.[31] Spectra recorded from inversion recovery, Hahn echo, and DgcsteSL_cc sequences were processed in vNMRJ (v. 3.2).

2.4. Molecular Dynamics Simulation of NaOH Solution. MD simulations were performed with the DLPOLY Classic software.[32] Cubic simulation boxes were composed of 453 H_2O molecules, 147 Na^+ and 147 OH^- ions. The interactions within the solution were represented by a polarizable force field. Polarization was treated by a core−shell model,[33] in which shells were integrated via an adiabatic process.[34] Mixed Lennard-Jones parameters were determined through the Lorentz−Berthelot rule.[35,36] At this high concentration, a pressure of 30 katm was necessary to maintain the density close to its experimental value. Simulations were carried out in the *NPT* ensemble with a Nosé−Hoover barostat and thermostat with a temperature of 293.15 K. Further details are given in Supporting Information Section S3.

3. RESULTS

3.1. Incoherent Elastic Intensity Scans. The temperature dependence of elastic intensity scans provides a quantitative measurement to determine the onset of transitions in the dynamics, that is, the temperatures at which the dynamics of H-bearing scatters (here H_2O, OH− $Al(OH)_4^-$ and Al-clusters) enter the time window of the spectrometer (determined by its energy resolution), leading to a decrease of the elastic intensity (Figure 1). The onset temperature of the

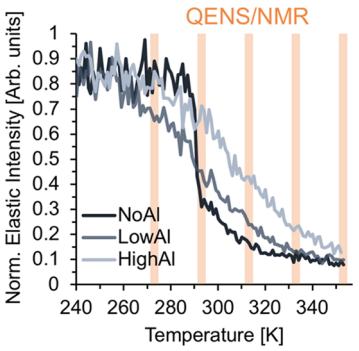

Figure 1. Normalized incoherent elastic intensity scans of the three studied solutions. Normalization is based on intensities at 10 K. Data collected at Q = 1.5 Å^{-1} are shown. The scans at other Q values gave similar results. The five vertical lines indicate the temperatures at which QENS and ^{1}H NMR measurements were performed.

dynamic transition is approximately Q-independent. As shown in Figure 1, the NaOH solution (NoAl) shows a sharp intensity drop at 290 K, which is in excellent agreement with the established liquids of the solution.[37,38] In comparison, the two NaOH−$NaAl(OH)_4$−H_2O solutions (LowAl and HighAl) exhibit somewhat less well-defined transitions at temperatures ∼260−270 K, below which the molecular motions start to slow down and reach a maximum plateau region down to the lowest temperature investigated. Both of these solutions, especially the LowAl sample, show weak kinks in the elastic intensity near the NaOH·2H_2O freezing temperature (∼290 K).[39] These are indicative of phase separation and subsequent freezing of certain phases (most likely NaOH·2H_2O), while the other species still retain mobility. On the high-temperature end of the spectra, the elastic scans for the two aluminate solutions still show an ongoing transition, indicating that species could be mobile at even higher temperatures. In general, adding aluminum in concentrated NaOH solutions suppresses the freezing transition in the bulk form, and the extent to which the dynamics slow down seems to be strongly dependent on the aluminate concentrations in the studied system.

3.2. ^{1}H NMR Spectroscopy. When salts are dissolved in water, the solution becomes more viscous, lengthening the diffusive−rotational relaxation times of ion-bound water and increasing dynamic inhomogeneity because of ion solvation.[40,41] At extremely high concentrations (in our description, higher than 10 *m*), the water-in-salt scenario applies, interionic attractions become significant, and solvent-shared ion associations are necessary to compensate for the decreased fraction of free H_2O. This, as would be expected in terms of packing effects alone, incurs extended connectivity of ion−solvent and solute clustering networks, and local structural "trapping" effects. The collective motion of the solutions occurring over long-time scales was probed via ^{1}H DOSY-NMR, which incorporates spatially dependent pulsed magnetic field gradients to measure the diffusion. Example spectra are shown in Figure S4, and the diffusion coefficients are listed in Table 2. This technique is also sensitive to the severely

DOI: 10.1021/acs.jpcb.8b09375
J. Phys. Chem. B XXXX, XXX, XXX−XXX

Table 2. Diffusion Coefficients, D (in 10^{-10} m^2 s^{-1}) and Rotational Correlation Time, τ (in ps) Acquired via ^{1}H NMR Spectroscopy[a]

	NoAl		LowAl		HighAl	
T (K)	D [10^{-10} m^2 s^{-1}]	τ [ps]	D [10^{-10} m^2 s^{-1}]	τ [ps]	D [10^{-10} m^2 s^{-1}]	τ [ps]
273	0.122(1)	610(80)	<0.390(2)	1430(130)	<0.219(1)	2770(360)
293	0.704(2)	184(14)	0.390(2)	253(8)	0.219(1)	308(9)
313	1.862(20)	129(8)	1.196(3)	165(12)	0.789(4)	219(3)
333	3.906(24)	132(7)	2.586(79)	142(5)	1.881(5)	190(3)
353	7.054(19)	161(18)	5.013(14)	151(3)	3.433(6)	192(6)

[a]The standard deviation values are shown in parenthesis. Diffusion coefficients denoted with lesser than (<) could not be measured because of a combination of very fast relaxation and slow diffusion coefficients.

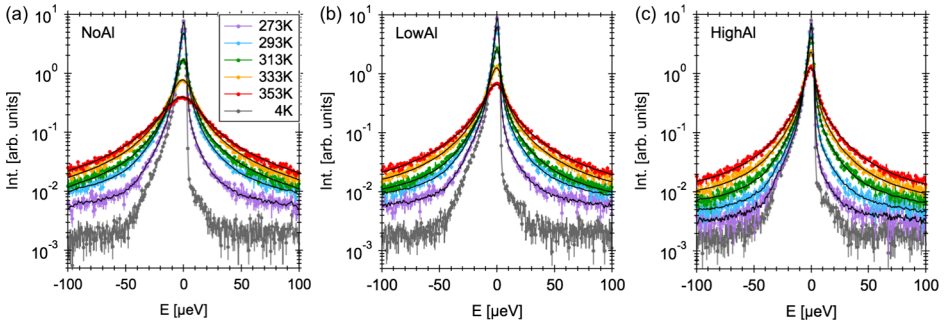

Figure 2. (a–c) Example of QENS spectra analysis for the three solutions at different temperatures and at Q = 0.7 Å^{-1}. The spectra in gray correspond to the experimental resolution function. The color dots represent the experimental spectra, while the black lines represent the fitting curves (individual Q-dependent fits) using eqs 1 and 2. See Figure S5 in Supporting Information Section S5 for the fits at other Q values.

restricted motions of OH^-, H_2O, $Al(OH)_4^-$, and Al-clusters compared to those expected from bulk water. In the NoAl solution, the observed diffusion coefficient varies from 0.122(1) m^2 s^{-1} at 273 K to 7.054(19) m^2 s^{-1} at 353 K. At room temperature, the observed diffusion coefficient of 0.704(2) m^2 s^{-1} is over 30 times slower than that of bulk water and is in good agreement with expected trends based on the enhanced viscosity.[42] In comparison, the LowAl and HighAl exhibits even slower collective motions. At 273 K, the translational dynamics could not be measured for either Al-containing solutions via DOSY-NMR. At higher temperatures, the observed diffusion coefficient was reduced for both LowAl and HighAl. These results suggest that (1) the signals originating from $Al(OH)_4^-$ exhibit reduced mobility compared to H_2O and OH^- and that (2) the water solvating the ions in these aluminate solutions also exhibits restricted motion compared to the NoAl solution. We note that the diffusion NMR measurement is weighted by relaxation processes occurring throughout the measurement, and that the measurement is biased toward the fast moving components, exhibiting slow spin lattice and transverse relaxation.[43−45]

Hahn echo and inversion recovery NMR pulse sequences were utilized to enable quantification of ensemble rotational correlation times, describing molecular reorientation on picosecond timescales. NMR measurements correspond to average relaxation properties of all species with labile ^{1}H ($Al(OH)_4^-$, Al-clusters, OH^-, and H_2O). Proton exchange between these species is rapid on the NMR timescale at all investigated temperatures, which is evident from the one observable resonance. Because of rapid exchange and long timescales, we do not attempt to deconvolute the observed relaxation into a fast and slow component, and instead look at the collective relaxation process. The effects of chemical confinement on ensemble ^{1}H rotational correlation times were revealed by proton spin lattice relaxation and transverse relaxation measurements, analyzed with Bloembergen–Purcell–Pound theory,[46] described in Supporting Information Section S4. The rotational correlation times increase from 600 to 2800 ps (increasing with [Na^+] and [Al^{3+}]) at 273 K to 150–200 ps at 353 K (Table 2).

3.3. QENS Spectra and Data Analysis. A representative description of the temperature-dependent QENS spectra is given in Figure 2a–c, where an abrupt change in the spectral line shape occurs between 273 and 293 K in NoAl and LowAl solutions. Such a change corresponds to the dynamic transition behavior revealed by the elastic scan data shown in Figure 1. The QENS signal from the HighAl solution is less temperature-dependent and reveals a significant slowing of the dynamics, in agreement with DOSY-NMR results. We fit experimental dynamic structure factor, $S(Q,E)$, using equations[47,48]

$$S(Q,E) = R(Q,E) \otimes [A_E(Q)\delta(E) + A_n(Q)L_n(Q,E) + A_b(Q)L_b(Q,E)] + BG \quad (1)$$

$$L_i(Q,E) = \frac{1}{\pi}\frac{\Gamma_i(Q)}{E^2 + \Gamma_i(Q)^2} \quad (2)$$

where $R(Q,E)$ is the resolution function of the BASIS spectrometer, $\delta(E)$ is the delta function centered at zero energy transfer, $L_n(Q,E)$ and $L_b(Q,E)$ are Lorentzian functions, and BG describes a linear background. $A_E(Q)$, $A_n(Q)$, and $A_b(Q)$ are the areas of elastic, narrow, and wide Lorentzians, respectively. The functional form of $L_i(Q,E)$ is by no means unique, but is a way to extract average relaxation times for a system with complex dynamics. The fitting procedure for all data sets were carried out by using (a) the PAN program in the DAVE[49] software package for the *individual* Q-dependent fit,

DOI: 10.1021/acs.jpcb.8b09375
J. Phys. Chem. B XXXX, XXX, XXX–XXX

and (b) the QClimax[50] program for the *global* Q-dependent fit. The difference between these two fitting procedures are described by the power law Q-dependence of peak width $\Gamma_i(Q)$ (half-width at half-maximum) for each relaxation procedure, that is, $\Gamma_i(Q) = \Gamma_i^o Q^{\lambda_i}$. In the *global* fitting, λ_i is a single fit parameter that characterizes the linewidth for all Q values (as a *global* feature) at each measured temperature. In the *individual* fitting, λ_i is not defined, instead *individual* $\Gamma_i(Q)$ is a free parameter, and the resulting Q-dependence of the linewidth contains certain degrees of variation when plotted as ln Γ_i versus ln Q. Table S3 summarizes the Γ_i^o values and Q-dependence of the slope λ_i from the two fitting procedures and Figures S6 and S7 highlight the Q-dependence of peak width $\Gamma_i(Q)$ at selected temperatures (see Supporting Information Section S5).

A meaningful comparison can be made on the basis of the λ value. For $\lambda = 2$, the standard Brownian diffusion is recovered, whereas $\lambda < 2$ indicates a localized diffusive character, often found in polymeric networks, glass-forming systems, and supercooled liquids.[51] It is observed that $\lambda = 2$ is not attained even at the highest temperatures explored (Table S3). The temperature dependence of the relaxation times, obtained from the Lorentzian Γ_i^o, as $\tau_i = \hbar/\Gamma_i^o$, is plotted in Figure 3 and summarized in Table 3 ($\hbar$ is the reduced Planck's constant). It should be noted that we did not make assumptions concerning the origin of particular components. Both fast (τ_b) and slow (τ_n) components probed by BASIS exhibit Arrhenius-type temperature dependence and show a similar trend between the two fits (Figure 3).

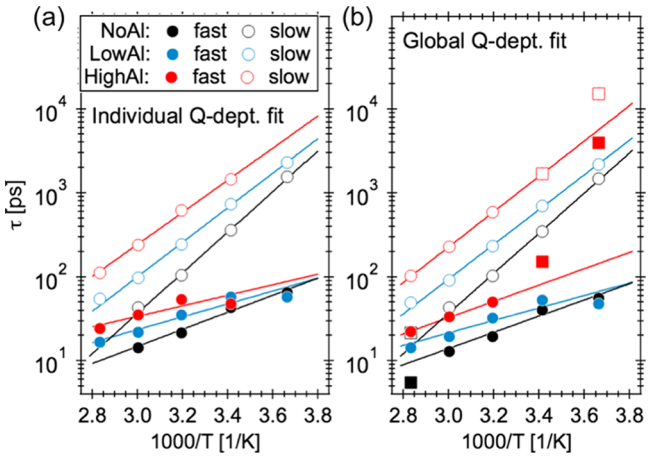

Figure 3. Temperature dependence of the relaxation times. Results obtained from the (a) individual and (b) global Q-dependent fit are given. The fast components (from Γ_b^o) are shown in closed circles and slow components (from Γ_n^o) are open circles. The Arrhenius fits of the two components (solid lines) yields activation energies, which are summarized in Table 3. In Figure 3a, the 353 K ($x = 2.83$) data points in NoAl, and the 273 K ($x = 3.66$) data points in HighAl were not shown because successful QENS fits cannot be achieved. In Figure 3b, the black squared data points at 353 K ($x = 2.83$) in NoAl, and the red squared data points at 293 K ($x = 3.41$) and 273 K ($x = 3.66$) in HighAl represent undefined errors because of the unsuccessful QENS fits. Error bars are smaller than the symbols for all data points. The temperature dependence of the relaxation times are rather similar, regardless of the data fitting approach used, thus providing additional reassurance of the validity of our results.

4. DISCUSSION

4.1. Complex Local Diffusive and Relaxation Process.

The emergence of anomalous transport in concentrated electrolytes is ubiquitous in nature. One prominent feature common to many of these systems is that they are densely packed, suggesting that slow and collective motions may be generic.[52] All solutions studied here follow the water-in-salt concept, if we take water coordination numbers (in the first solvation shell) for Na^+, OH^-, and $Al(OH)_4^-$ ions to be 5–6,[1,6] 3–5,[21,26] and 8–12,[27,53] respectively, and consider a much weaker water affinity of $Al(OH)_4^-$ anions in comparison with Na^+ and OH^- ions (simply based on the charge densities of ions). The H_2O/ion ratios summarized in Table 1 clearly indicates the deficiency of water molecules, directing OH^- in the primary coordination sphere of Na^+, and the formation of extended H_2O-solvent and/or OH^--ligand shared Na^+–$Al(OH)_4^-$ polyhedral structures. A schematic representation of these networks in 20 *m* NaOH solution was obtained by classical MD simulations. The networks are shown in Figure 4 to illustrate the extended structure and complex coordination environments at high salt concentrations.

Time correlation functions were computed, using the simulated 20 *m* NaOH solution illustrated in Figure 4, to track: (1) Na^+–OH^- ion-pair dynamics; and (2) events where H_2O leaves the first solvation shell of Na^+. The decay of each type of interaction follows a triexponential behavior, as indicated in Figure 5. At the short-time scales (<100 ps), the Na^+–OH^- interactions exhibit two components (1.7 and 10.8 ps), which are faster than the two components (2.6 and 23.5 ps) observed in Na^+–H_2O interactions. The 1 to 3 ps motions likely correspond to unsuccessfully exchange attempts, typically occurring on the order of 1–2 ps.[55,56] At long-time scales, the opposite trend is observed, where some Na^+–OH^- interactions exhibit much longer decay times than Na^+–H_2O interactions, as evidenced by a significant fraction of stable Na^+–OH^- ion pairs throughout the duration of the simulation. Although the time correlation functions given in Figure 5 consider all the different possible arrangements of OH^- and H_2O around Na^+ ions, identification of the exact OH^- and H_2O exchange mechanisms that contribute to the analyzed timescales is lost. This is because significant fractions of OH^- and H_2O molecules are bridged between two or more Na^+ ions, as evident from previous work.[22–24] Therefore, the corresponding kinetics and exchange mechanisms should not be the same as their exchange around a single Na^+ ion. Thus, significant subensemble analyses of the Na^+–OH^- and Na^+–H_2O coordination polyhedra are required to fully understand the molecular contributions to the dynamics, which is beyond of the scope of the current work.

On the basis of the water-in-salt concept and the Q-dependence of the two Lorentzian Γ_i components (Table S3 and Figure S6), the data are interpreted in terms of the local structural relaxation. The broader component is attributed to the local relaxation, or fast motions in the transient local environment (because its Q-dependence is flatter), and the narrow component is attributed to the slow restricted diffusion (because its Q-dependence is steeper and $\lambda_n < 2$). These two components should be strongly coupled. The effects of the two motions are best resolved at low temperatures, like a supercooled liquid approaching a glass transition, in which the rotational (fast) and translational (slow) molecular motions are decoupled.[51] At higher temperatures, many

DOI: 10.1021/acs.jpcb.8b09375
J. Phys. Chem. B XXXX, XXX, XXX–XXX

Table 3. Relaxation Times τ_i (in ps) and Activation Energies (kJ/mol) from the Two fitting Procedures[a]

	individual		individual		individual	
	NoAl		LowAl		HighAl	
	slow: τ_n	fast: τ_b	slow: τ_n	fast: τ_b	slow: τ_n	fast: τ_b
			T (K)			
273	1559(9)	65.5(9)	2298(14)	57.6(9)		
293	361(1)	43.5(5)	742(4)	58.9(4)	1466(7)	47.6(8)
313	104.2(6)	21.7(4)	245(1)	35.3(3)	623(3)	54.1(5)
333	43.1(4)	14.2(4)	97(1)	21.8(2)	242(1)	35.5(3)
353			54(1)	16.6(2)	112(1)	24.4(2)
			E_a			
	46.4(1)	19.5(3)	39.5(1)	14.7(1)	36.6(1)	12.0(2)
	global		global		global	
	NoAl		LowAl		HighAl	
	slow: τ_n	fast: τ_b	slow: τ_n	fast: τ_b	slow: τ_n	fast: τ_b
			T (K)			
273	1490(8)	56.0(8)	2193(14)	48.1(9)	15 295	3971
293	349(1)	40.3(4)	702(3)	53.4(5)	1704	153
313	103(1)	19.3(4)	231(1)	32.6(3)	588(3)	50.5(5)
333	43.1(3)	12.9(5)	91.3(7)	19.6(3)	227(1)	33.3(2)
353	21.4	5.5	49.2(6)	14.4(2)	103(1)	22.4(3)
			E_a			
	45.9(1)	18.5(3)	39.7(1)	14.3(2)	40.4(2)	18.6(3)

[a]The standard deviation values are shown in parenthesis. Numbers without standard deviations in the global fitting procedure represent undefined errors because of unsuccessful QENS fits.

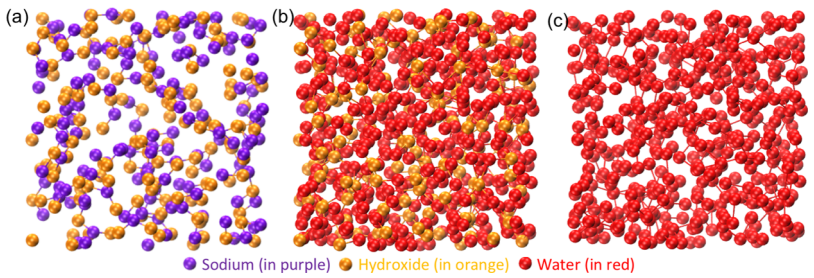

Figure 4. Three-dimensional representation of the network of (a) Na^+−OH^- ion−ion interactions, (b) OH^-−H_2O ion−water interactions, and (c) H_2O−H_2O water−water interactions. These layers of intermolecular networks are obtained from MD simulation at 20 *m* NaOH with the network analysis using ChemNetworks.[54] Na^+ ions are in purple spheres, OH^- in orange spheres, and H_2O molecules in red spheres. See Supporting Information Section S3 for a description of the MD simulation and details of the network analysis.

types of motion across different timescales are activated and superimposed, leading to cooperative nondiffusional dynamics. In the temperature and timescales of the QENS experiments investigated, we do not observe normal diffusive motions, where the mean-squared displacement of mobile species would be a linear function of time. In contrast, complementary ^1H DOSY-NMR data reveal the ensemble motions of protonated species and indicate that the normal diffusive behavior occurs on the microsecond timescale by the invariance of the diffusion coefficient to the duration between spatially dependent gradient pulses. Accordingly, the slow QENS component (on the order of 350−750 ps at 293 K; Table 3 and Figure 3) observed here cannot simply be caused by a reduction in free movement. The underlying physical processes are complex and differ to the self-diffusion (vehicular-type) ion/water transport mechanisms.[57] The slow QENS component is thought to comprise the collective diffusion of more than one species, each moving with its own diffusion coefficient, causing conformational changes to the liquid structure in many stages within the polymeric clustering network (i.e., structural diffusion).[41,52,58] Raman spectroscopy of the LowAl solution (Figure S1) shows that the Al concentration in our studied solutions is sufficient to form higher order species. The temperature-resolved structural evolution of the HighAl solution, obtained from elastic neutron total scattering/radial distribution function analysis (see Figure S2), shows very little structural change (other than normal Debye−Waller thermal broadening) with increasing temperatures up to 348 K, which is consistent with attributing the slow component to overall localized/restricted motions in these densely packed solution systems. It should be noted that, while the mechanisms underlying the translational microscopic dynamics of the mobile species in our samples are collective in character, our QENS measurements are predominantly sensitive to the single-particle component of the microscopic dynamics of the mobile species, because of the very high incoherent neutron scattering cross-section of protons.

On the other hand, the observed QENS fast relaxations on the order of 40−60 ps at 293 K (Table 3 or Figure 3) can be qualitatively correlated to the continuous lifetime of the

DOI: 10.1021/acs.jpcb.8b09375
J. Phys. Chem. B XXXX, XXX, XXX−XXX

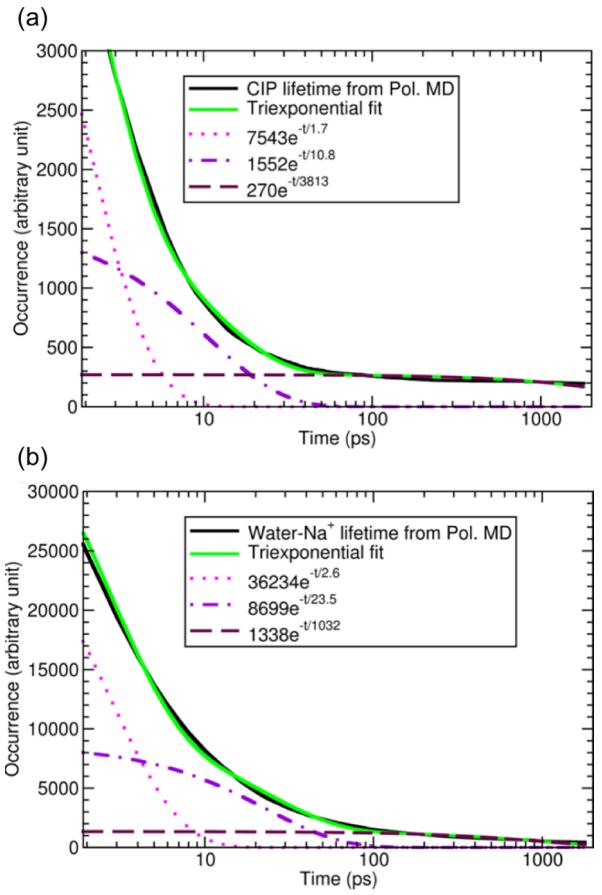

Figure 5. Time correlation functions $C(t)$ calculated for time <2000 ps by averaging over all possible origins for (a) OH^- ions and (b) H_2O molecules that were in the first solvation shell around Na^+ in 20 *m* NaOH solution. A triexponential decay function is used for the fit and the approximation of residence times. More information is given in the Supporting Information, Section S3.

formation of large hydrated ion clusters beyond simple contact ion pairs. The local motion of these solvated clusters likely exhibits backbone "tumbling" or "frame reorientations" of the intact bonds in the solute species and the solvating water molecules. Marcus[2] reviewed the subject, considering the ion pairs present in the electrolyte solution, and estimating an ion-pairing relaxation time on the order of 100−200 ps, which is superimposed on the water relaxation time on the order of 1−20 ps. Here, the present fast QENS component and NMR ensemble rotational correlation times are compared with dielectric relaxation spectra (DRS) of Buchner et al.[59] of concentrated $NaAl(OH)_4$ solutions. As shown in Figure 6, DRS of concentrated $NaAl(OH)_4$ solutions quantified the slowing of water solvent Cole−Cole relaxation-time distribution from 8.27 ps in bulk water up to 66 ps in the concentrated brines and resolved an additional low frequency Debye dispersion with a relaxation time of 60−200 ps, assigned to solute-related relaxation processes. The increase in NMR rotational correlation times with increasing $[Al^{3+}]$ is consistent with the results of this study, and both NMR and DRS data fall into the time window of the QENS components for the relaxation (or minimum formation lifetime) related to the solvated clusters. In the DRS study, the solute-related relaxation processes is assigned (by Buchner et al.[59] and Sipos[14]) to solvent separated, $Na^+-[(HO)_3Al-O-Al-(OH)_3]^{2-}$ ion pairs for the simplest explanation. However, more complex ion association and local structural rearrangements cannot be ruled out.

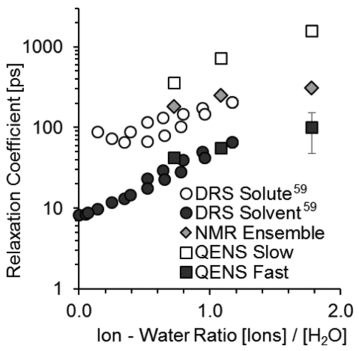

Figure 6. Comparison of QENS relaxation times (square), NMR rotational correlation times (diamond), and dielectric relaxations times (circles)[59] of sodium aluminate solutions as a function of ion water ratio at 293 K. The QENS data points represent the averaged relaxation times from the two fitting procedures (individual and global *Q*-dependent fits).

4.2. Comparison to Confined H_2O Motions in Other Systems. It is important to realize that QENS signals, weighted by motions of H_2O, are about 5.5, 8.9, and 5.5 times stronger than excess OH^- ions in the NoAl, LowAl, and HighAl solutions, respectively, and are about 4.7 and 2.9 times larger than $Al(OH)_4^-$ species in LowAl and HighAl solutions, respectively. If we considered that the QENS signals are dominated by motions of H_2O, the residence times and activation energies of the H_2O motions can be compared with other systems, especially in terms of the fast relaxation processes of local origin. Such systems include molecular layers of water at mineral−water interfaces and aqueous solutions confined in porous media. Dynamics of H_2O molecules sorbed on rutile (TiO_2) surfaces[60] are a good comparison because the system has been studied on the same spectrometer and analyzed in a similar way using two Lorentzian functions. Arrhenius temperature dependence with activation energy of about 9.0 kJ/mole is reported for H_2O reorientation events on rutile, and the residence time of this fast relaxation is about 24 ps at 280 K.[60] The system also possesses a non-Arrhenius temperature-dependent, slow component with a residence time of 178 ps at 280 K, which is related to the translational jumps between surface-bound and unbound states. Here, for the fast QENS relaxation processes, we observe a substantially slower residence time in all three solutions, for example, in the NoAl solution, the relaxation times of the fast component are ∼40 ps at 293 K (Table 3 and Figure 3). The activation energies of the fast component are also much higher than the value of 9.0 kJ/mole determined for H_2O reorientation on rutile, and they are about 19, 15, and 12 kJ/mole in NoAl, LowAl, and HighAl solutions, respectively (Table 3). The faster water dynamics and non-Arrhenius behaviors for water loosely bound on rutile, in comparison, indicate that H_2O molecules in the NoAl, LowAl, and HighAl solutions are under greater confinement.

When compared to pure water, the relaxation time of hindered isotropic rotational jumps at 293 K is 1.25 ps (or 3.75 ps if not assumed isotopically) and has Arrhenius behavior with an activation energy of 7.74 kJ/mole.[61] This picosecond reorientation corresponds well to water jump models predicted by classical MD (3.3−3.6 ps at 300 K).[62] In contrast, various

DOI: 10.1021/acs.jpcb.8b09375
J. Phys. Chem. B XXXX, XXX, XXX−XXX

MD simulations have estimated a mean retention time of 10–40 ps at 300 K for H_2O exchanges between the first and second solvation shells around Na^+.[4,7,23,40] Different from the approach demonstrated in Figure 5, Hellström and Behler,[23] using their developed neural network-based MD, performed detailed analyses for both H_2O and OH^- exchanges around a *single* Na^+ solvation shell. In a fully saturated NaOH solution (27.7 *m* at 300 K), they estimated a substantial increase in retention time for both H_2O molecules (53 ps) and OH^- ions (29 ps) around a single Na^+ solvation shell.[23] Because Na^+ has higher affinity for H_2O than for OH^-,[24] the rate-limiting step for OH^- and H_2O exchange around Na^+ is determined by the direct H_2O leaving events. The system also exhibits proton transfer-driven H_2O/OH^- exchange events, for which the timescale of water deprotonation (while still bound to Na^+) decreases significantly from about 167 ps at 1 *m* (a rare event) to 31 ps at 27.7 *m* (about a third of water self-exchange is induced by proton transfer).[23] The characteristic relaxation times of the fast QENS components studied here (on the order of 40–60 ps at 293 K) certainly differ from that in the bulk water or the simplest H_2O self-exchange around a single Na^+ in dilute aqueous solution. This supports the interpretation that the complexity in the results obtained here originates from cluster dynamics and confined water motions, although the estimated residence times for H_2O or OH^- exchange events around a single Na^+ (either through the direct or proton-transfer-driven pathways) at high NaOH concentration is somewhat comparable to the current observations, that is, 28–53 ps at 300 K from neural network-based MD versus ~40 ps at 293 K from QENS. To what extent the direct or proton transfer-driven pathways proceeded to longer timescales (>100 ps) or involve more than one Na^+ ion as an extended network of clusters, remains unclear, as does the pronounced slowdown when $Al(OH)_4^-$ oxyanions are introduced into the system. For other superconcentrated electrolytes (e.g. LiTFSI, EMITFSI, H_2SO_4, etc.), it has been suggested phenomenologically (via a modified Vogel–Fulcher–Tammann model) that the mechanism of even nonproton transport can transition from vehicular to a correlated ion mechanism through multidimensional solvent–solute networks,[12,57] and our findings are consistent with this description.

5. CONCLUSIONS

The microscopic dynamics of Na-based electrolyte solutions ($NaOH_{(aq)}$ and $NaAl(OH)_{4(aq)}$) at high concentrations have been investigated using ^1H NMR and QENS techniques. The temperature dependence of normal translational diffusion at microsecond timescales and ensemble rotational correlation times on the order of 184–300 ps at 293 K for H-bearing species ($Al(OH)_4^-$, OH^-, and H_2O) has been shown by ^1H NMR. ^1H NMR studies also revealed that an increase in Al and Na concentration corresponded to: (i) a reduction in translocation; and (ii) slower ensemble rotation correlation times. QENS measurements, on the other hand, reveal two local relaxation processes on the timescale of 40–60 and 350–750 ps at 293 K. On the basis of the *Q*-dependence of the two Lorentzian components, the fast component agrees with ^1H NMR rotational correlation times and the reported DRS solute relaxation times. This fast QENS component is thus assigned to the relaxation processes (or minimum lifetime) related to the solvated cluster motions, likely a restricted backbone-like motion. The slow component likely comprises the collective diffusion, reflecting the complex underlying physical processes that occur in a densely packed solution system. Both fast and slow QENS relaxation processes show Arrhenius-type temperature dependence and are strongly coupled at elevated temperatures. Because of the presence of an extended network structure and the complexity of the coordination in high salt environments, analysis of the self-exchange events of H_2O, OH^-, and $Al(OH)_4^-$ coordinated to the Na^+ ion are insufficient to represent the underlying dynamics. Instead, the majority of the H-bearing species are bridged by two or more Na^+ ions, and there is a high propensity for the formation of dimers or polynuclear $Al(OH)_4^-$ complexes. The exact molecular origin of the observed timescales and activation energies remains unclear and requires further theoretical investigation to unravel the three-, four- and many-body reaction pathways that exist in these highly concentrated water-in-salt electrolyte solutions and go beyond the simple ion solvation/pairing events that have been well studied in dilute systems.

■ ASSOCIATED CONTENT

Supporting Information

The Supporting Information is available free of charge on the ACS Publications website at DOI: 10.1021/acs.jpcb.8b09375.

Raman spectroscopy, neutron total scattering/radial distribution function analysis, classical MD simulations, ^1H NMR analysis, and QENS data analysis (PDF)

■ AUTHOR INFORMATION

Corresponding Authors

*E-mail: trenton.graham@pnnl.gov (T.R.G.).
*E-mail: wangh3@ornl.gov (H.-W.W.).

ORCID

Trent R. Graham: 0000-0001-8907-8004
Eugene Mamontov: 0000-0002-5684-2675
Katharine Page: 0000-0002-9071-3383
Aurora Clark: 0000-0001-9381-721X
Carolyn I. Pearce: 0000-0003-3098-1615
Andrew G. Stack: 0000-0003-4355-3679
Hsiu-Wen Wang: 0000-0002-2802-4122

Notes

The authors declare no competing financial interest.

■ ACKNOWLEDGMENTS

This research was supported by IDREAM (Interfacial Dynamics in Radioactive Environments and Materials), an Energy Frontier Research Center funded by the U.S. Department of Energy (DOE), Office of Science, Basic Energy Sciences (BES). NMR experiments were performed using the facilities at the Environmental Molecular Science Laboratory (EMSL), a national scientific user facility sponsored by the DOE Office of Biological and Environmental Research (BER) at the Pacific Northwest National Laboratory (PNNL). PNNL is a multiprogram national laboratory operated for DOE by Battelle Memorial Institute under contract no. DE-AC05-76RL0-1830. Research at the BASIS and NOMAD beamlines at Spallation Neutron Source (SNS), Oak Ridge National Laboratory (ORNL) was sponsored by the Scientific User Facilities Division, BES, DOE. Work by A.R.C. and the QClimax software were made available through ICE-MAN: Integrated Computational Environment, Modeling and Analysis of Neutron data (LDRD 8237) project, funded by the

DOI: 10.1021/acs.jpcb.8b09375
J. Phys. Chem. B XXXX, XXX, XXX–XXX

Laboratory Directed Research and Development program at ORNL.

REFERENCES

(1) Ohtaki, H.; Radnai, T. Structure and Dynamics of Hydrated Ions. *Chem. Rev.* **1993**, *93*, 1157−1204.

(2) Marcus, Y. Effect of Ions on the Structure of Water: Structure Making and Breaking. *Chem. Rev.* **2009**, *109*, 1346−1370.

(3) Bakker, H. J. Structural Dynamics of Aqueous Salt Solutions. *Chem. Rev.* **2008**, *108*, 1456−1473.

(4) Obst, S.; Bradaczek, H. Molecular Dynamics Study of the Structure and Dynamics of the Hydration Shell of Alkaline and Alkaline-Earth Metal Cations. *J. Phys. Chem.* **1996**, *100*, 15677−15687.

(5) Mancinelli, R.; Botti, A.; Bruni, F.; Ricci, M. A.; Soper, A. K. Hydration of Sodium, Potassium, and Chloride Ions in Solution and the Concept of Structure Maker/Breaker. *J. Phys. Chem. B* **2007**, *111*, 13570−13577.

(6) Mähler, J.; Persson, I. A Study of the Hydration of the Alkali Metal Ions in Aqueous Solution. *Inorg. Chem.* **2012**, *51*, 425−438.

(7) Kelley, M.; Donley, A.; Clark, S.; Clark, A. Structure and Dynamics of NaCl Ion Pairing in Solutions of Water and Methanol. *J. Phys. Chem. B* **2015**, *119*, 15652−15661.

(8) Zhang, Q.; Wu, T.; Chen, C.; Mukamel, S.; Zhuang, W. Molecular Mechanism of Water Reorientational Slowing down in Concentrated Ionic Solutions. *Proc. Natl. Acad. Sci. U.S.A.* **2017**, *114*, 10023−10028.

(9) Choi, J.-H.; Choi, H. R.; Jeon, J.; Cho, M. Ion Aggregation in High Salt Solutions. VII. The Effect of Cations on the Structures of Ion Aggregates and Water Hydrogen-Bonding Network. *J. Chem. Phys.* **2017**, *147*, 154107.

(10) Reichenbach, J.; Wynne, K. Frustration vs Prenucleation: Understanding the Surprising Stability of Supersaturated Sodium Thiosulfate Solutions. *J. Phys. Chem. B* **2018**, *122*, 7590−7596.

(11) Sosso, G. C.; Chen, J.; Cox, S. J.; Fitzner, M.; Pedevilla, P.; Zen, A.; Michaelides, A. Crystal Nucleation in Liquids: Open Questions and Future Challenges in Molecular Dynamics Simulations. *Chem. Rev.* **2016**, *116*, 7078−7116.

(12) Suo, L.; Borodin, O.; Gao, T.; Olguin, M.; Ho, J.; Fan, X.; Luo, C.; Wang, C.; Xu, K. "Water-in-salt" electrolyte enables high-voltage aqueous lithium-ion chemistries. *Science* **2015**, *350*, 938−943.

(13) Hind, A. R.; Bhargava, S. K.; Grocott, S. C. The Surface Chemistry of Bayer Process Solids: A Review. *Colloid. Surface. Physicochem. Eng. Aspect.* **1999**, *146*, 359−374.

(14) Sipos, P. The structure of Al(III) in strongly alkaline aluminate solutions—A review. *J. Mol. Liq.* **2009**, *146*, 1−14.

(15) Donald, I. W.; Metcalfe, B. L.; Taylor, R. N. J. The Immobilization of High Level Radioactive Wastes Using Ceramics and Glasses. *J. Mater. Sci.* **1997**, *32*, 5851−5887.

(16) Zapałowski, M.; Bartczak, W. M. Structural and Dynamical Properties of Concentrated Aqueous NaOH Solutions: A Computer Simulation Study. *Comput. Chem.* **2000**, *24*, 459−468.

(17) Chen, B.; Park, J. M.; Ivanov, I.; Tabacchi, G.; Klein, M. L.; Parrinello, M. First-Principles Study of Aqueous Hydroxide Solutions. *J. Am. Chem. Soc.* **2002**, *124*, 8534−8535.

(18) Botti, A.; Bruni, F.; Imberti, S.; Ricci, M. A.; Soper, A. K. Solvation of Hydroxyl Ions in Water. *J. Chem. Phys.* **2003**, *119*, 5001−5004.

(19) Botti, A.; Bruni, F.; Imberti, S.; Ricci, M. A.; Soper, A. K. Ions in Water: The Microscopic Structure of Concentrated NaOH Solutions. *J. Chem. Phys.* **2004**, *120*, 10154−10162.

(20) Megyes, T.; Bálint, S.; Grósz, T.; Radnai, T.; Bakó, I.; Sipos, P. The Structure of Aqueous Sodium Hydroxide Solutions: A Combined Solution x-Ray Diffraction and Simulation Study. *J. Chem. Phys.* **2008**, *128*, 044501.

(21) Mandal, A.; Tokmakoff, A. Vibrational Dynamics of Aqueous Hydroxide Solutions Probed Using Broadband 2DIR Spectroscopy. *J. Chem. Phys.* **2015**, *143*, 194501.

(22) Hellström, M.; Behler, J. Concentration-Dependent Proton Transfer Mechanisms in Aqueous NaOH Solutions: From Acceptor-Driven to Donor-Driven and Back. *J. Phys. Chem. Lett.* **2016**, *7*, 3302−3306.

(23) Hellström, M.; Behler, J. Proton-Transfer-Driven Water Exchange Mechanism in the Na^+ Solvation Shell. *J. Phys. Chem. B* **2017**, *121*, 4184−4190.

(24) Hellström, M.; Behler, J. Structure of Aqueous NaOH Solutions: Insights from Neural-Network-Based Molecular Dynamics Simulations. *Phys. Chem. Chem. Phys.* **2017**, *19*, 82−96.

(25) Hassanali, A.; Giberti, F.; Cuny, J.; Kühne, T. D.; Parrinello, M. Proton Transfer through the Water Gossamer. *Proc. Natl. Acad. Sci. U.S.A.* **2013**, *110*, 13723−13728.

(26) Tuckerman, M. E.; Marx, D.; Parrinello, M. The Nature and Transport Mechanism of Hydrated Hydroxide Ions in Aqueous Solution. *Nature* **2002**, *417*, 925−929.

(27) Pouvreau, M.; Dembowski, M.; Clark, S. B.; Reynolds, J. G.; Rosso, K. M.; Schenter, G. K.; Pearce, C. I.; Clark, A. E. Ab Initio Molecular Dynamics Reveal Spectroscopic Siblings and Ion Pairing as New Challenges for Elucidating Prenucleation Aluminum Speciation. *J. Phys. Chem. B* **2018**, *122*, 7394−7402.

(28) Mamontov, E.; Herwig, K. W. A Time-of-Flight Backscattering Spectrometer at the Spallation Neutron Source, BASIS. *Rev. Sci. Instrum.* **2011**, *82*, 085109.

(29) Neuefeind, J.; Feygenson, M.; Carruth, J.; Hoffmann, R.; Chipley, K. K. The Nanoscale Ordered MAterials Diffractometer NOMAD at the Spallation Neutron Source SNS. *Nucl. Instrum. Methods Phys. Res. Sect. B Beam Interact. Mater. Atoms* **2012**, *287*, 68−75.

(30) Raiford, D. S.; Fisk, C. L.; Becker, E. D. Calibration of Methanol and Ethylene Glycol Nuclear Magnetic Resonance Thermometers. *Anal. Chem.* **1979**, *51*, 2050−2051.

(31) Callaghan, P. T.; Le Gros, M. A.; Pinder, D. N. The Measurement of Diffusion Using Deuterium Pulsed Field Gradient Nuclear Magnetic Resonance. *J. Chem. Phys.* **1983**, *79*, 6372−6381.

(32) Smith, W.; Forester, T. R. *Dl_poly Classic*, Version 1.10; Stfc Daresbury Laboratory,c Daresbury: Warrington Wa4 4ad.E, 2015.

(33) Dick, B. G.; Overhauser, A. W. Theory of the Dielectric Constants of Alkali Halide Crystals. *Phys. Rev.* **1958**, *112*, 90−103.

(34) Lamoureux, G.; Harder, E.; Vorobyov, I. V.; Roux, B.; MacKerell, A. D. A Polarizable Model of Water for Molecular Dynamics Simulations of Biomolecules. *Chem. Phys. Lett.* **2006**, *418*, 245−249.

(35) Lorentz, H. A. Ueber Die Anwendung Des Satzes Vom Virial in Der Kinetischen Theorie Der Gase. *Ann. Phys.* **1881**, *248*, 127−136.

(36) Berthelot, D. Sur Le Mélange Des az. *C. R. Hebd. Séances Acad. Sci.* **1898**, *126*, 1703−1855.

(37) Linke, W. F. Solubilities. *Inorganic and Metal Organic Compounds: A Compilation of Solubility Data from the Periodical Literature*; Van Nostrand: Washington D.C., 1965; Vol. 2.

(38) Pickering, S. U. LXI.-The hydrates of sodium, potassium, and lithium hydroxides. *J. Chem. Soc. Trans.* **1893**, *63*, 890−909.

(39) Siemens, P. R.; Giauque, W. F. The Entropies of the Hydrates of Sodium Hydroxide. II. Low-Temperature Heat Capacities and Heats of Fusion of $NaOH{\cdot}2H_2O$ and $NaOH{\cdot}3.5H_2O$. *J. Phys. Chem.* **1969**, *73*, 149−157.

(40) Turton, D. A.; Hunger, J.; Hefter, G.; Buchner, R.; Wynne, K. Glasslike Behavior in Aqueous Electrolyte Solutions. *J. Chem. Phys.* **2008**, *128*, 161102.

(41) Ren, G.; Chen, L.; Wang, Y. Dynamic Heterogeneity in Aqueous Ionic Solutions. *Phys. Chem. Chem. Phys.* **2018**, *20*, 21313−21324.

(42) Sipos, P. M.; Hefter, G.; May, P. M. Viscosities and Densities of Highly Concentrated Aqueous MOH Solutions ($M^+ = Na^+, K^+, Li^+, Cs^+, (CH_3)_4N^+$) at 25.0°C. *J. Chem. Eng. Data* **2000**, *45*, 613−617.

(43) Price, W. S.; Tsuchiya, F.; Arata, Y. Time Dependence of Aggregation in Crystallizing Lysozyme Solutions Probed Using NMR Self-Diffusion Measurements. *Biophys. J.* **2001**, *80*, 1585−1590.

DOI: 10.1021/acs.jpcb.8b09375
J. Phys. Chem. B XXXX, XXX, XXX−XXX

(44) Price, W. S. Pulsed-Field Gradient Nuclear Magnetic Resonance as a Tool for Studying Translational Diffusion: Part II. Experimental Aspects. *Concepts Magn. Reson* **1998**, *10*, 197−237.
(45) Virk, A. S.; Stait-Gardner, T.; Willis, S. A.; Torres, A. M.; Price, W. S. Macromolecular Crowding Studies of Amino Acids Using NMR Diffusion Measurements and Molecular Dynamics Simulations. *Front. Physiol.* **2015**, *3*, 1−15.
(46) Bloembergen, N.; Purcell, E. M.; Pound, R. V. Relaxation Effects in Nuclear Magnetic Resonance Absorption. *Phys. Rev.* **1948**, *73*, 679−712.
(47) Mamontov, E. Diffusion in Confinement as a Microscopic Relaxation Mechanism in Glass-Forming Liquids. *Chem. Phys. Lett.* **2012**, *530*, 55−60.
(48) Mamontov, E.; Yue, Y.; Bahadur, J.; Guo, J.; Contescu, C. I.; Gallego, N. C.; Melnichenko, Y. B. Hydration Level Dependence of the Microscopic Dynamics of Water Adsorbed in Ultramicroporous Carbon. *Carbon* **2017**, *111*, 705−712.
(49) Azuah, R. T.; Kneller, L. R.; Qiu, Y.; Tregenna-Piggott, P. L. W.; Brown, C. M.; Copley, J. R. D.; Dimeo, R. M. DAVE: A Comprehensive Software Suite for the Reduction, Visualization, and Analysis of Low Energy Neutron Spectroscopic Data. *J. Res. Natl. Inst. Stand. Technol.* **2009**, *114*, 341−358.
(50) Bahadur, J.; Contescu, C. I.; Ramirez-Cuesta, A. J.; Mamontov, E.; Gallego, N. C.; Cheng, Y.; Daemen, L. L.; Melnichenko, Y. B. Properties of Immobile Hydrogen Confined in Microporous Carbon. *Carbon* **2017**, *117*, 383−392.
(51) Zanotti, J.-M.; Bellissent-Funel, M.-C.; Chen, S.-H. Relaxational Dynamics of Supercooled Water in Porous Glass. *Phys. Rev. E: Stat. Phys., Plasmas, Fluids, Relat. Interdiscip. Top.* **1999**, *59*, 3084−3093.
(52) Höfling, F.; Franosch, T. Anomalous Transport in the Crowded World of BiologicalCells. *Rep. Prog. Phys.* **2013**, *76*, 046602.
(53) Tossell, J. A. Theoretical Studies on Aluminate and Sodium Aluminate Species in Models for Aqueous Solution: $A1(OH)_3$, $Al(OH)_4^-$, and $NaAl(OH)_4$. *Am. Mineral.* **1999**, *84*, 1641−1649.
(54) Ozkanlar, A.; Clark, A. E. ChemNetworks: A Complex Network Analysis Tool for Chemical Systems. *J. Comput. Chem.* **2014**, *35*, 495−505.
(55) Stack, A. G.; Rustad, J. R. Structure and Dynamics of Water on Aqueous Barium Ion and the {001} Barite Surface. *J. Phys. Chem. C* **2007**, *111*, 16387−16391.
(56) Rey, R.; Hynes, J. T. Hydration Shell Exchange Kinetics: An MD Study for $Na^+_{(Aq)}$. *J. Phys. Chem.* **1996**, *100*, 5611−5615.
(57) Yim, C.-H.; Tam, J.; Soboleski, H.; Abu-Lebdeh, Y. On the Correlation between Free Volume, Phase Diagram and Ionic Conductivity of Aqueous and Non-Aqueous Lithium Battery Electrolyte Solutions over a Wide Concentration Range. *J. Electrochem. Soc.* **2017**, *164*, A1002−A1011.
(58) Marx, D.; Chandra, A.; Tuckerman, M. E. Aqueous Basic Solutions: Hydroxide Solvation, Structural Diffusion, and Comparison to the Hydrated Proton. *Chem. Rev.* **2010**, *110*, 2174−2216.
(59) Buchner, R.; Sipos, P.; Hefter, G.; May, P. M. Dielectric relaxation of concentrated alkaline aluminate solutions. *J. Phys. Chem. A* **2002**, *106*, 6527−6532.
(60) Mamontov, E.; Wesolowski, D. J.; Vlcek, L.; Cummings, P. T.; Rosenqvist, J.; Wang, W.; Cole, D. R. Dynamics of Hydration Water on Rutile Studied by Backscattering Neutron Spectroscopy and Molecular Dynamics Simulation. *J. Phys. Chem. C* **2008**, *112*, 12334−12341.
(61) Teixeira, J.; Bellissent-Funel, M.-C.; Chen, S. H.; Dianoux, A. J. Experimental determination of the nature of diffusive motions of water molecules at low temperatures. *Phys. Rev. A: At., Mol., Opt. Phys.* **1985**, *31*, 1913−1917.
(62) Laage, D.; Stirnemann, G.; Sterpone, F.; Rey, R.; Hynes, J. T. Reorientation and Allied Dynamics in Water and Aqueous Solutions. *Annu. Rev. Phys. Chem.* **2011**, *62*, 395−416.

DOI: 10.1021/acs.jpcb.8b09375
J. Phys. Chem. B XXXX, XXX, XXX−XXX